**E. David Bell**
Department of Bioengineering,
University of Utah,
Salt Lake City, UT 84112

**Matthew Converse**
Department of Mechanical Engineering,
University of Utah,
Salt Lake City, UT 84112

**Haojie Mao**
Telemedicine and Advanced Technology
Research Center,
Department of Defense Biotechnology High
Performance Computing Software
Applications Institute,
U.S. Army Medical Research and
Materiel Command,
Frederick, MD 21702

**Ginu Unnikrishnan**
Telemedicine and Advanced Technology
Research Center,
Department of Defense Biotechnology High
Performance Computing Software
Applications Institute,
U.S. Army Medical Research and
Materiel Command,
Frederick, MD 21702

**Jaques Reifman**
Telemedicine and Advanced Technology
Research Center,
Department of Defense Biotechnology High
Performance Computing Software Applications
Institute,
U.S. Army Medical Research and
Materiel Command,
Frederick, MD 21702

**Kenneth L. Monson**[1]
Department of Bioengineering,
University of Utah,
Salt Lake City, UT 84112;
Department of Mechanical Engineering,
University of Utah,
1495 E. 100 S., MEK 1550,
Salt Lake City, UT 84112
e-mail: ken.monson@utah.edu

# Material Properties of Rat Middle Cerebral Arteries at High Strain Rates

*Traumatic brain injury (TBI), resulting from either impact- or nonimpact blast-related mechanisms, is a devastating cause of death and disability. The cerebral blood vessels, which provide critical support for brain tissue in both health and disease, are commonly injured in TBI. However, little is known about how vessels respond to traumatic loading, particularly at rates relevant to blast. To better understand vessel responses to trauma, the objective of this project was to characterize the high-rate response of passive cerebral arteries. Rat middle cerebral arteries (MCAs) were isolated and subjected to high-rate deformation in the axial direction. Vessels were perfused at physiological pressures and stretched to failure at strain rates ranging from approximately 100 to 1300 $s^{-1}$. Although both in vivo stiffness and failure stress increased significantly with strain rate, failure stretch did not depend on rate.* [DOI: 10.1115/1.4039625]

*Keywords: traumatic brain injury, blast injury, blood vessel mechanical properties, high strain rate testing*

## Introduction

Traumatic brain injury (TBI) claims approximately 1.7 million victims each year in the U.S., approximately 50,000 of whom die [1]. Patients who survive the initial trauma are frequently left with debilitating neurologic deficits. Total annual costs of TBI in the U.S. have been estimated at $60 billion [2]. While the frequency of injury in the U.S. has recently remained relatively constant year-to-year, the global incidence of TBI continues to increase dramatically [3]. TBI has also become a serious problem in the military, where a significant fraction of brain injuries is associated with blast exposure [4,5]. Blast-induced TBI includes injury mechanisms not typically associated with civilian TBI [6,7].

The cerebral vessels play an important role in the maintenance of a healthy brain. Although damage to brain tissue is the fundamental concern in TBI, nearly all significant TBIs include some element of injury to the blood vessels [8,9], and any injury or dysfunction of the vasculature places neural tissue at risk. Hemorrhage and other forms of vascular dysfunction, such as vasospasm, appear to play a particularly prominent role in blast-induced TBI [10,11].

Despite the frequency of vessel damage in TBI and the significant role of vessels in the recovery of brain tissue, little is known about the deformations that vessels undergo during trauma or about the mechanisms governing their response to this loading. Although computational models can effectively predict the motion of the brain during trauma, the previous attempts to include

---

cerebral blood vessels in such models have been limited [12–14]. One reason for this is the lack of data defining cerebral vessel response at high strain rates, particularly those relevant to blast loading. Such properties need to be defined for computational models to be meaningful.

The previous investigations of strain rate effects in blood vessels have included tests on the aorta, carotid artery, and cerebral arteries and veins from both humans and animals (see previous summary [15]). Findings on the significance of strain rate are mixed, but those reporting a measurable effect have typically found that ultimate stress increases and ultimate strain decreases with increasing strain rate. A number of these tests were conducted on cerebral vessels [16–21]. However, only one study investigated response to strain rates thought to be relevant to blast, and it was limited to bridging veins [16].

Motivated by an ultimate interest in developing a computational model of brain-vessel loading in blast, the objective of this study was to characterize the strain rate dependence of cerebral arteries in the rat, which is commonly used as an animal model of TBI. We hypothesized that perfused rat middle cerebral arteries (MCAs) are sensitive to high strain rates. The primary mode of vessel loading during TBI is not known. However, we expect that vessels rotate to align their axes with imposed deformation and thus sought to characterize their response in the axial direction. Results from high-rate tests were compared to our previous quasi-static findings on rat MCA properties [22].

## Materials and Methods

**Specimen Dissection and Preparation.** A total of 61 MCA segments were dissected from 11 male Sprague Dawley rats ($360.9 \pm 41.4$ g). All procedures met requirements established by the Institutional Animal Use and Care Committee at the University of Utah and the Animal Care and Use Review Office at the U.S. Army Medical Research and Materiel Command, Ft. Detrick, MD. Rats were anesthetized with isoflurane and exsanguinated via cardiac perfusion, using Hank's Buffered Saline Solution (HBSS; KCl 5.37, KH2PO4 0.44, NaCl 136.9, Na2HPO4 0.34, D-Glucose 5.55, NaHC03 4.17; concentrations in mM), followed by a 1% nigrosin dye (Sigma-Aldrich, St. Louis, MO) HBSS solution. The dye enhanced visibility of the artery and its branches during dissection. Where possible, multiple samples were obtained from each animal. MCA side branches were ligated with individual fibrils from unwound 6-0 silk suture, and the vessel was cannulated with glass tip needles and secured with 11-0 monofilament suture. Lack of calcium in the HBSS ensured a passive response.

**Testing Apparatus and Procedure.** Each specimen was subjected to two stages of testing. In the first, the vessel was preconditioned, and the reference configuration was established. In the second, the specimen was stretched rapidly in the axial direction.

*Preconditioning*: Similar to the work described previously [23], the MCA was mounted horizontally in a physiological saline solution (PSS) bath and tied to two needles with 11-0 monofilament sutures. Tests were performed at room temperature. The bath included a glass window in its base for light and a submersible glass viewing window above the specimen. One needle held stationary during testing was mounted to a 250 g capacity load cell (model 31 Low, Honeywell, Golden Valley, MN) through an *X–Y* stage for fine adjustments in needle alignment. During preconditioning, the other needle was mounted to a low-friction sled connected to a voice coil actuator that controlled axial stretch of the MCA. Actuator position was given by a digital encoder (resolution 1.0 $\mu$m). A digital video camera mounted to a light microscope recorded vessel deformations during testing. The MCA was pressurized with PSS originating from a syringe pump. The fluid path passed through the proximal needle, mounted MCA, and distal needle to a closed valve that prevented flow.

Inline pressure transducers were located both proximal and distal to the mounted MCA, equidistant from the vessel. The average of the pressures measured at these two transducers was taken to be the pressure inside the MCA or the luminal pressure. Data and video were captured at 100 and 3 Hz, respectively.

The sample was preconditioned by quasi-statically oscillating the luminal pressure from 6.7 to 20.0 kPa (50–150 mmHg) for five cycles while holding the axial stretch constant. This was initially done at a low axial stretch level (barely taut) and subsequently repeated at gradually higher stretch until the in vivo length was identified as the length where the axial force remained constant as the luminal pressure increased [24]. All vessels experienced a maximum axial stretch of approximately 1.1 times the in vivo length during preconditioning. Following preconditioning, the vessel was stretched, while unpressurized, from a buckled state to 1.1 times the in vivo length while monitoring the axial force. The reference length was identified as the length at which the axial force began to increase from zero.

*High-rate testing*: For high-rate tests, the syringe pump was replaced with a simple water column to maintain constant pressure, and the voice coil actuator was set at a position where the vessel was slightly buckled. The attached low-friction sled was then locked into place with a frangible set screw and disconnected from the actuator. The PSS was removed from the bath immediately before testing to eliminate any drag associated with the subsequent displacement. High-rate motion was achieved by dropping a weight down a fixed tube into a padded, metal cup. One end of a steel cable was attached to the cup, while the other was connected to the low-friction sled, with a pulley in between to transform vertical motion into horizontal displacement (Fig. 1). The frangible set screw was a standard 10-24 screw with a blind hole drilled in the end for the placement of the tip of a toothpick. The toothpick prevented preliminary motion of the sled but easily broke free when the force from the cable was applied. A high-speed video camera (Phantom Miro EX4; Vision Research, Perth, Australia) recorded vessel deformations. Sled motion was arrested, after vessel stretch, by a rigid stop at the end of the track; maximum travel of the sled was well above that associated with vessel failure. Rate of stretch was adjusted by changing the drop height to target low ($100\,\mathrm{s}^{-1}$), medium ($500\,\mathrm{s}^{-1}$), and high ($1000\,\mathrm{s}^{-1}$) strain-rate values. Vibrations associated with cup impact were reduced and delayed (so as to not appear in the load cell signal until after the stretching event) by padding the cup and by mounting the load cell on a cork block. Pressures were maintained at either 6.7 or 13.3 kPa (50 or 100 mmHg). Data and video were acquired at 100,000 and 30,000 Hz, respectively. For the highest target strain rate ($1000\,\mathrm{s}^{-1}$), this typically produced ten images between the reference length and the length corresponding to the previously measured [22] mean failure stretch ratio of $\lambda_z = 1.35 \pm 0.08$. High speed camera image resolution was 95 pix/mm.

**Data Processing.** Noise observed in the load cell readings was smoothed using the SAE J211 filter [25]. Based on the previous research conducted by our group [26], it was known that high-rate loading, even at small levels of force, has the potential to excite a load cell's structure and to produce oscillations in its output that do not accurately represent the force applied to the load cell. To remove any such confounding data from the high-rate axial tests, the load cell and the attached fixture were modeled as a linear mass-spring-damper system that was excited by the force produced by the blood vessel (Fig. 2).

To define parameters for this model, the spring constant $k$ was calculated as the ratio of the specified full scale load and deflection for the load cell. The solution of the differential equation governing the system was then fit to data from a ringing test, where the sensor was excited by a small impulse, to estimate the damping coefficient $b$ and the effective mass $m$ (combined mass of movable portion of load cell, fixture, and needle). The governing differential equation, its solution for free response to an impulse,
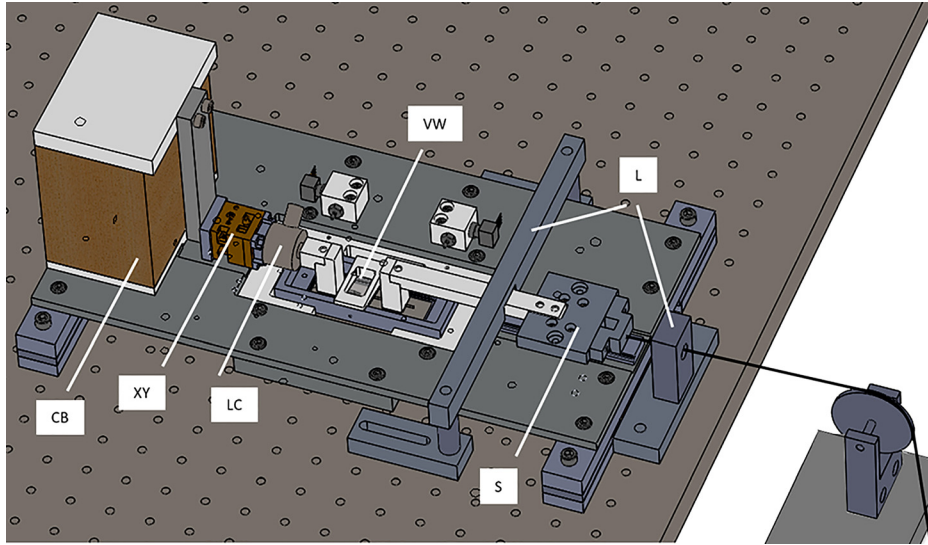
**Fig. 1  Schematic of the high-rate testing apparatus. Vessel deformation was observed through a viewing window (VW). The left end of the vessel was fixed to the stationary load cell (LC), which was mounted to a vibration-damping cork base (CB) through an *X–Y* positioning stage (XY). The right end of the vessel displaced rapidly when the sled (S) was accelerated by the steel cable extending to the base of the drop tube (not shown). Rigid limits (L) were imposed to bound movement of the sled and prevent damage to the apparatus.**

and the damped natural frequency $\omega_d$ are given by Eqs. (1a)–(1c), respectively,

$$m\ddot{x} + b\dot{x} + kx = F_{BV} \tag{1a}$$

$$x = x_0 e^{-\frac{b}{2m}t}\sin(\omega_d t + \varphi) \tag{1b}$$

$$\omega_d = \sqrt{\frac{k}{m} - \left(\frac{b}{2m}\right)^2} \tag{1c}$$

where $x$ is the displacement of the unfixed end of the load cell, $F_{BV}$ is the force of the blood vessel, and $x_0$ is the initial displacement in a ringing test. With the system parameters defined, the transfer function between the output ($F_{LC} = b\dot{x} + kx$) and input ($F_{BV}$) forces was determined using Laplace transformation as $G = F_{LC}/F_{BV} = (cs + k)/(ms^2 + cs + k)$. This transfer function was then inverted, and the input $F_{BV}$ of the system was predicted from the measured output $F_{LC}$, using the *lsim* command in MATLAB (MathWorks, Natick, MA). Prior to simulation with *lsim*, the inverse transfer function was multiplied by a low-pass filter with a high frequency to add additional poles to the system and allow use of *lsim* without influencing system behavior. The predicted input was then used in a forward simulation with the noninverted transfer function to confirm that the process was reversible. Results showed that there was a delay between the input and output forces, particularly at high rates of loading (Fig. 2), so all measured force signals were transformed as described.

Predictions of the transform were subsequently validated by coupling a piezoelectric force transducer (208C01, PCB Piezotronics, Depew, NY) to the blood vessel side of the load cell, allowing direct measurement of the force imposed on the load cell during testing. For these tests, the transform was modified to account for associated changes in system mass and ringing frequency. Results showed good correlation between predicted and measured values under a variety of loading conditions (Fig. 2).

Owing to the high speeds of the axial tests, otherwise subtle lags in signal transfer resulted in significant misalignments between image and force data. Therefore, we decided to align the force and image data so that the peak force coincided with the image immediately prior to the start of visual disruption of the

sample. This naturally included time shift errors as large as the time between frames (0.033 ms).

The resulting data were used to determine the Cauchy stress-stretch response. Vessels were assumed to be homogeneous circular cylinders, with axial stretch defined by the below equation:
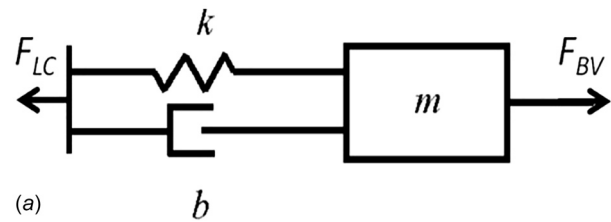


(a)
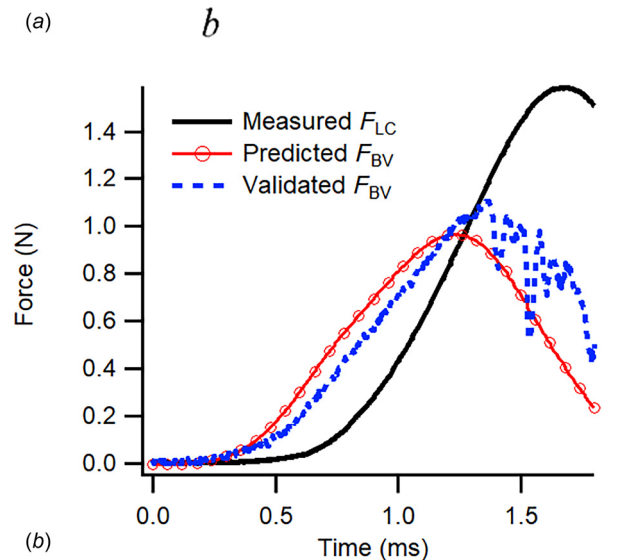


(b)

**Fig. 2  (a) Diagram of mass-spring-damper system used to model load cell. Applied load from blood vessel ($F_{BV}$) is to the right; output load ($F_{LC}$) is to the left. (b) Force-time plot of vessel force predicted by reverse simulation in a representative medium strain rate test ($\sim$500 s$^{-1}$). The predicted vessel force was subsequently validated through direct measurement using a piezoelectric force transducer.**

$$\lambda_z = \left(\frac{l}{L}\right) \tag{2}$$

where $l$ is the current length and $L$ is the reference length determined following preconditioning. Application of Newton's law results in the mean axial Cauchy stress, as defined in the below equation:

$$T_z = \frac{\lambda_z}{A}\left(F_z + \frac{\pi}{4}p_i d_i^2 - \hat{m}a\right) \tag{3}$$

where $A$ is the reference cross-sectional area, $F_z$ is the experimentally measured axial force, $p_i$ is the internal pressure, $d_i$ is the current inner diameter, $\hat{m}$ is vessel segment mass, and $a$ is its acceleration. The inertial term was found to be negligible relative to the measured force. Residual stresses were not considered given the large variation observed in opening angle when vessel rings were cut and allowed to open. Because the current inner diameter could not be measured, it was approximated by assuming incompressibility, as shown in the below equation:

$$d_i = \sqrt{d_o^2 - 4A/(\pi\lambda_z)} \tag{4}$$

where $d_o$ is the current outer diameter. Reference cross-sectional area $A$ was measured from images (498 pix/mm) of cross sections taken from the ends of vessel segments prior to testing. Mean circumferential Cauchy stress $T_\theta$ was defined as shown in the below equation:

$$T_\theta = p_i\left(\frac{d_i}{d_o - d_i}\right) \tag{5}$$

Stress-stretch data around approximate in vivo conditions were examined. Axial in vivo length was determined for each sample by observing the pressure-axial force response during preconditioning tests [24]. In vivo stiffness was defined by fitting an exponential function through the data around the in vivo stretch and calculating the value of the derivative at the in vivo stretch. Note that stiffness is used here as a measure of the resistance of the vessel structure to deformation, rather than as an intrinsic tissue property. Failure stress was determined as the highest stress achieved during testing. For comparisons with the previously reported data, this quantity was calculated as the first Piola–Kirchhoff (first P-K) stress—the current force divided by the reference cross-sectional area. Failure stretch was defined as the value of the stretch ratio at the peak first P-K stress value.

**Statistical Analysis.** High-rate data were initially separated into six groups, one for each combination of rate and pressure, with either 10 or 11 samples each. The similarity of variances for these six groups was confirmed with a Levene test. In vivo stiffness and failure values were then analyzed with a one-way analysis of variance (ANOVA) test, followed by a two-way t-test. Although the statistical threshold was set as $p < 0.05$ for the ANOVA test, the large number of groups resulted in a post-hoc statistical threshold of $p < 0.0083$ following a Bonferroni correction. Because this analysis showed that pressure was not significantly influential, further analysis considered rate groups only, composed of data from tests at both pressure levels. We also examined differences between the high-rate groups and the previously collected quasi-static data (obtained from male Sprague–Dawley rats of similar weight) [22]. With the inclusion of these additional data, the Levene test indicated that some variances between groups were not similar. Therefore, statistical comparison was accomplished with Welch's ANOVA test ($p < 0.05$) followed by a Tukey–Kramer post-hoc test. Because Tukey–Kramer tests do not give a specific $p$-value (they use a calculated q-statistic compared with a critical q-statistic based on the initial
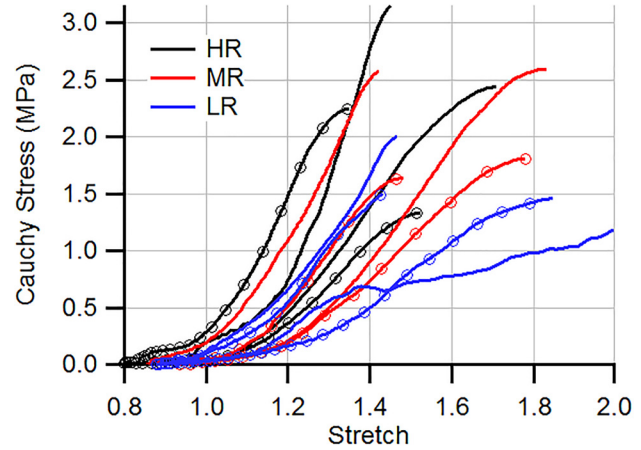


Fig. 3 Representative axial Cauchy stress-stretch curves for all groups, including high (>700 s$^{-1}$; HR), medium (400–500 s$^{-1}$; MR), and low (100–200 s$^{-1}$; LR) strain rate cases. The internal pressure was fixed at 6.7 kPa for specimens indicated by open circles; for all others, it was fixed at 13.3 kPa. These representative cases suggest trends toward higher stresses and lower stretches with higher strain rates; there is no apparent effect of pressure.

$p < 0.05$ threshold), specific $p$-values for individual comparisons are not reported. Rather, post-hoc significance levels for individual comparisons are simply specified as significant or not significant. A Bonferroni correction was also used for these Tukey–Kramer tests, resulting in a statistical threshold of $p < 0.0125$ for the basis of the critical q-statistic. Multiple samples were obtained from each animal but were divided among the three rate groups for testing to avoid any animal-specific influence.

## Results

A total of 61 samples were successfully tested. Mean ($\pm$stdev) unloaded vessel diameter and tested length were 0.26 ($\pm$0.03) and 0.92 ($\pm$0.11) mm, respectively. Stress-stretch curves showed the typical nonlinear response seen in quasi-static extension tests on soft tissue (Fig. 3), including previous experiments on rat MCA [22]. However, results included more scatter than is typically seen during quasi-static tests. Qualitative evaluation of the curves suggested a possible dependence on strain rate, as increasing the rate appeared to increase stress for a given stretch. Applied strain rates
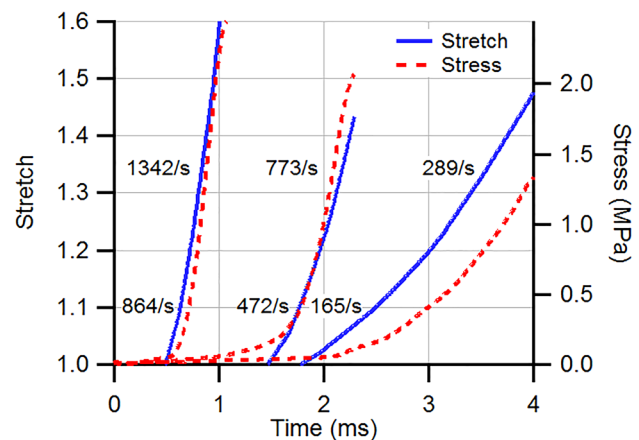


Fig. 4 Stretch and Cauchy stress as a function of time for representative cases. Strain rates are indicated over in vivo (1.05–1.15) and large (1.30–1.40) stretch ranges for each stretch curve. These data show that the strain rate at the in vivo stretch was 60% of that at larger stretches.
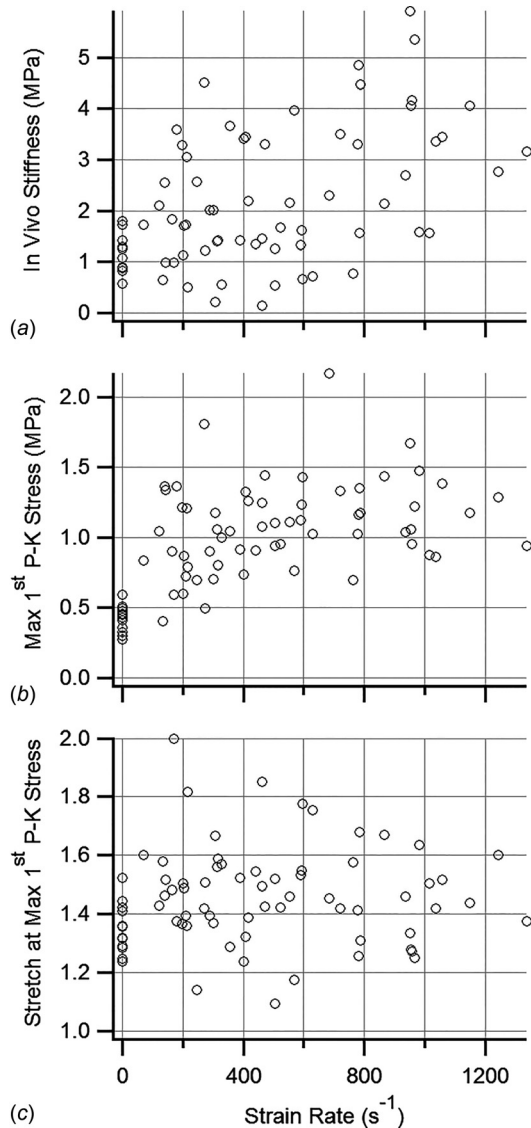
**Fig. 5** (*a*) In vivo stiffness, (*b*) Max first P-K stress (failure stress), and (*c*) stretch at maximum first P-K stress as a function of strain rate (calculated over the in vivo region), including quasi-static data from the previously reported experiments [22]. Despite the significant scatter, these plots show trends of increasing stiffness and failure stress with strain rate. Stretch at maximum stress appears to be independent of rate.

varied from approximately 100 to 1300 s$^{-1}$. As shown for representative cases in Fig. 4, the strain rate was not constant during testing, but each curve can still be reasonably approximated with a straight line. Rates at in vivo strains were approximately 60% of those at failure. All results are presented here in terms of the in vivo strain rate since the data are intended to inform simulation

of vessels initially at the in vivo configuration, but the potential dependence of failure values on the maximum strain rate was also evaluated.

As the stress-stretch curves suggest, plots of both in vivo stiffness and maximum first P-K stress indicate a dependence on strain rate (Fig. 5). This is particularly true with inclusion of the previously collected quasi-static data. Although there was significant scatter, these data suggest that in vivo stiffness generally increases with rate, whereas the maximum stress appears to increase less rapidly at high rates than at lower ones. In contrast, failure stretch did not appear to be influenced by strain rate. It is clear that the data from the present high-rate tests are significantly more scattered than those in previous quasi-static experiments.

As Fig. 5 shows, strain rates did not fall into distinct bins. Although three values were targeted, variability in specimen length and in the extent of pretest buckling led to a relatively continuous distribution of rates. Nevertheless, the data were categorized into three groups for statistical analysis (Table 1).

Upon sorting into six groups (two pressure values at each of three rates), one-way ANOVA indicated some differences ($p = 0.0154$), although post-hoc testing showed that the differences were only between groups differing in rate. Pressure was then removed as a variable, and a subsequent analysis was performed for the three rate groups (Low, Med, and High), whose group sizes were doubled because all specimens were included regardless of pressure. With this categorization, in vivo stiffness values from the high-rate group (High) were significantly different from those of both the medium (Med; $p = 0.0017$) and low (Low; $p = 0.0027$) rate groups, although there was no difference between the medium and low group values ($p = 0.8685$; Fig. 6; solid lines identify statistically different groups). The maximum first P-K stress values were also significantly different between the high- and low-rate groups ($p = 0.0049$), although no other comparisons were statistically different. Failure stretch did not differ among the three groups (ANOVA, $p = 0.7905$). The dependence of failure values on maximum strain rate demonstrated similar trends.

In an additional analysis, we included a fourth rate group consisting of previously collected quasi-static data on the same vessels. Because the variances for this group were generally smaller than those of the other groups, the analysis required the use of Welch's ANOVA followed by Tukey–Kramer post-hoc tests. Mean values of both in vivo stiffness and maximum stress increased by approximately a factor of three between the quasi-static values and the data collected at higher rates. Statistical tests on the four groups together revealed a significant difference in in vivo stiffness between the high-rate (High) group and all other groups, but there was no difference in in vivo stiffness among the other groups (Fig. 6; statistically different groups identified with dashed lines). For the maximum first P-K stress values, the low- (Low), medium- (Med), and high- (High) rate groups were different from the quasi-static group, although the difference between the High and Low groups did not persist. Quasi-static failure stretch values were not statistically different from those of any of the other groups. As was true for the three-group analysis, the maximum strain rate was shown to have some influence on failure stress but none on stretch at maximum stress.

**Table 1** Summary of the mean (±standard deviation) for strain rate and in vivo stiffness in each of the six axial test groups (*N* = 10 for all but one group)

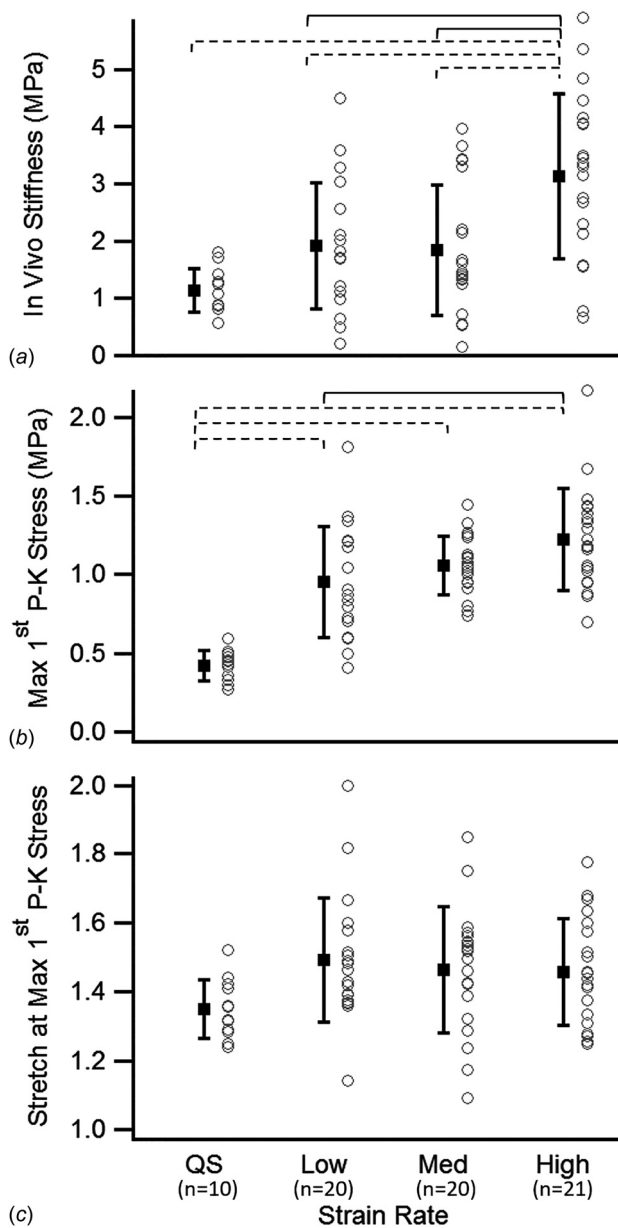| Rate group | High pressure (13.3 kPa) | | Low pressure (≤6.7 kPa) | |
| | Strain rate (s$^{-1}$) | In vivo stiffness (MPa) | Strain rate (s$^{-1}$) | In vivo stiffness (MPa) |
| --- | --- | --- | --- | --- |
| High (>700 s$^{-1}$) | 877±146 | 2.97±1.38 | 959±213[a] | 3.27±1.54[a] |
| Med (400–500 s$^{-1}$) | 443±98 | 2.04±1.02 | 479±95 | 1.66±1.26 |
| Low (100–200 s$^{-1}$) | 206±59 | 2.21±1.22 | 199±73 | 1.62±0.94 |

[a]Indicates the group where $N = 11$.

**Fig. 6** Mean (±standard deviation): (*a*) axial in vivo stiffness, (*b*) maximum first Piola–Kirchhoff (first P-K) stress, and (*c*) stretch at maximum first P-K stress for the quasi-static (QS), Low, Med, and High rate groups. Solid and dashed brackets indicate statistically different groups for the three- and four-group comparisons, respectively. These figures confirm statistically significant rate sensitivity for in vivo stiffness and failure stress but not for failure stretch.

## Discussion

The objective of this project was to characterize the mechanical response of rat cerebral arteries to high-rate axial stretch. Results show that in vivo stiffness and peak stress were both sensitive to increases in strain rate from quasi-static levels to over $1000 \, \text{s}^{-1}$. However, failure stretch did not change with strain rate.

Despite statistical confirmation that in vivo stiffness and maximum stress were both dependent on strain rate, it is interesting that their patterns of dependence were somewhat different. Specifically, the maximum stress was more sensitive to medium-level rates than in vivo stiffness. Only the highest rate (above $700 \, \text{s}^{-1}$) tests produced in vivo stiffness values that were statistically different from quasi-static values, whereas the largest difference in

maximum stress occurred between the quasi-static group and the lowest of the three high-rate groups. Because the mechanisms responsible for rate effects in soft tissues have not been defined, it is unclear whether the difference in rate dependence patterns for these parameters is due to some fundamental difference or is simply a result of data scatter that would be resolved with larger group sizes. It is clear, however, that the values of both parameters generally increased with strain rate.

Most studies have reported either increasing ultimate stress accompanied by decreasing ultimate strain or no change in either parameter [15]. Consistent with our finding, Mohan and Melvin [27] previously reported rate dependence of ultimate stress but not of ultimate strain in the aorta. It should be noted that the mechanisms responsible for rate dependence have not been defined, although it is common to consider the viscoelastic response of soft tissues to behave according to some version of the standard linear solid model. If this representation is accurate, increased stress would be expected at a given strain with increasing rate. However, because the standard linear solid model does not capture failure, it does not predict whether the failure strain would change. Further research on the mechanisms of rate dependence would help to better understand the effect of rate on failure stretch.

Strain rates from the current study ranged from approximately 100 to $1300 \, \text{s}^{-1}$ at the in vivo configuration. Because in vivo configuration rates were approximately 60% of the rates at larger deformations, values as high as approximately $2000 \, \text{s}^{-1}$ were studied at failure. Although the strain rates experienced by cerebral blood vessels during blast have not been quantified, the previous research here suggests that the range studied here is appropriate. Studies of both human cadavers [28] and inanimate models [29–31] have shown that brain tissue strain rates range from 10 to $100 \, \text{s}^{-1}$ in conventional TBI events. Ballistic strain rates in the brain have been reported as ranging between 1000 and $3000 \, \text{s}^{-1}$ [32]. However, blast-induced strains and strain rates have been more difficult to quantify, presumably because the strains under such loading are typically small [33]. But recent modeling efforts suggest that tissue strain rates appropriate to blast are on the order of hundreds per second [14,34,35]. The strain rates investigated here are considerably higher than those in most previous studies of blood vessels, although a few included rates over $100 \, \text{s}^{-1}$ [18,20,21,26], and one included a number of tests near $1000 \, \text{s}^{-1}$ [16]. The relatively high rates reported here were primarily possible because of the small size of the specimens, since a small-diameter vessel may be properly tested with a similarly small length [36].

It should be noted that the blood vessels in this study were perfused during testing. Lee and Haut [20], upon finding a lack of rate dependence in bridging veins, suggested that the inertia of blood inside a vessel may lead to rate dependence even if the tissue itself is not rate sensitive. This structural effect may play a role in the present findings. However, others have reported rate dependence in the absence of perfusion [15], so there appears to be some inherent material sensitivity to rate.

Experiments conducted at high rates are inherently noisy, as shown by the scatter in our results. This includes noise in the load cell due to vibrations associated with rapid accelerations, as well as in the imposed deformation. In our case, the vessels were buckled prior to extension to prevent them from stretching before the desired high rate had been achieved. Figure 4 shows that although this was largely successful, the strain rate generally continued to increase above the in vivo level. However, some of the scatter in our data is likely to be associated with variations in the amount of pretest buckling that was imposed. Despite our attempts to be consistent, small variations in this factor could have significantly influenced the results owing to the shortness of the specimens. Another likely contributor to the scatter is the process used to align the high-speed video-documented deformations with measurements of force. As noted in the Methods section, alignment of the force and image data based on evidence of specimen failure potentially resulted in time shift errors as large as $0.033 \, \text{ms}$ (the time between video frames).

An additional limitation of the present work is the lack of accounting for stress wave effects in the vessels as they were stretched. Given the high rates studied, it is likely that all portions of the vessel were not experiencing the same force and deformation as recorded by the load cell and video, even after adjustment of the load cell signal to account for the time of force transfer through the load cell. Future research at such rates could benefit from collecting video images at higher speeds to allow visualization of stress waves.

Because tests conducted at high rates have the potential to excite the natural frequency of a load cell, we used a simple model to remove any associated confounding data from the measured vessel force. Subsequent validation experiments showed that model-predicted values generally agreed with those measured directly using a force transducer that is better suited for dynamic loading. However, small discrepancies in predicted values likely contributed some variation to reported results.

In closing, our work shows that perfused rat middle cerebral arteries are sensitive to strain rates ranging from quasi-static to over $1000 \, \text{s}^{-1}$. However, this sensitivity is apparently limited to the stiffness of the vessel response and the ultimate stress, as failure stretch was not sensitive to strain rate. These data will allow the study of blood vessel loading during TBI through computational models.

## References

[1] Faul, M., Xu, L., Wald, M. M., and Coronado, V. G., 2010, "Traumatic Brain Injury in the United States: Emergency Department Visits, Hospitalizations and Deaths 2002-2006," Centers for Disease Control and Prevention, National Center for Injury Prevention and Control, Atlanta, GA, Report.

[2] Finkelstein, E., Corso, P. S., and Miller, T. R., 2006, *The Incidence and Economic Burden of Injuries in the United States*, Oxford University Press, New York.

[3] Maas, A. I. R., Stocchetti, N., and Bullock, R., 2008, "Moderate and Severe Traumatic Brain Injury in Adults," Lancet Neurol., **7**(8), pp. 728–741.

[4] Coupland, R. M., and Meddings, D. R., 1999, "Mortality Associated With Use of Weapons in Armed Conflicts, Wartime Atrocities, and Civilian Mass Shootings: Literature Review," BMJ, **319**(7207), pp. 407–410.

[5] Belmont, P. J., Jr., McCriskin, B. J., Sieg, R. N., Burks, R., and Schoenfeld, A. J., 2012, "Combat Wounds in Iraq and Afghanistan From 2005 to 2009," J. Trauma Acute Care Surg., **73**(1), pp. 3–12.

[6] Cullis, I. G., 2001, "Blast Waves and How They Interact With Structures," J. R. Army Med. Corps, **147**(1), pp. 16–26.

[7] Cernak, I., and Noble-Haeusslein, L. J., 2010, "Traumatic Brain Injury: An Overview of Pathobiology With Emphasis on Military Populations," J. Cereb. Blood Flow Metab., **30**(2), pp. 255–266.

[8] Graham, D. I., 1996, "Neuropathology of Head Injury," *Neurotrauma*, R. K. Nrayan, J. E. Wilberger, and J. T. Povlishock, eds., McGraw-Hill, New York, pp. 43–59.

[9] DeWitt, D., and Prough, D. S., 2003, "Traumatic Cerebral Vascular Injury: The Effects of Concussive Brain Injury on the Cerebral Vasculature," J. Neurotrauma, **20**(9), pp. 795–825.

[10] Armonda, R. A., Bell, R. S., Vo, A. H., Ling, G., DeGraba, T. J., Crandall, B., Ecklund, J., and Campbell, W. W., 2006, "Wartime Traumatic Cerebral Vasospasm: Recent Review of Combat Casualties," Neurosurgery, **59**(6), pp. 1215–1225.

[11] DeWitt, D. S., and Prough, D. S., 2009, "Blast-Induced Brain Injury and Posttraumatic Hypotension and Hypoxemia," J. Neurotrauma, **26**(6), pp. 877–887.

[12] Zhang, L., Bae, J., Hardy, W. N., Monson, K. L., Manley, G. T., Goldsmith, W., Yang, K. H., and King, A. I., 2002, "Computational Study of the Contribution of the Vasculature on the Dynamic Response of the Brain," Stapp Car Crash J., **46**, pp. 145–164.

[13] Ho, J., and Kleiven, S., 2007, "Dynamic Response of the Brain With Vasculature: A Three-Dimensional Computational Study," J. Biomech., **40**(13), pp. 3006–3012.

[14] Mao, H., Zhang, L., Jiang, B., Genthikatti, V. V., Jin, X., Zhu, F., Makwana, R., Gill, A., Jandir, G., Singh, A., and Yang, K. H., 2013, "Development of a Finite Element Human Head Model Partially Validated With Thirty Five Experimental Cases," ASME J. Biomech. Eng., **135**(11), p. 111002.

[15] Stemper, B. D., Yoganandan, N., and Pintar, F. A., 2007, "Mechanics of Arterial Subfailure With Increasing Loading Rate," J. Biomech., **40**(8), pp. 1806–1812.

[16] Löwenhielm, P., 1974, "Dynamic Properties of the Parasagittal Bridging Veins," Z. Rechtsmed., **74**(1), pp. 55–62.

[17] Löwenhielm, P., 1978, "Dynamic Strain Tolerance of Blood Vessels at Different Post-Mortem Conditions," J. Bioeng., **2**, pp. 509–515.

[18] Delye, H., Goffin, J., Verschueren, P., Vander Sloten, J., Van der Perre, G., Alaerts, H., Verpoest, I., and Berckmans, D., 2006, "Biomechanical Properties of the Superior Sagittal Sinus-Bridging Vein Complex," Stapp Car Crash J., **50**, pp. 625–636.

[19] Chalupnik, J., Daly, C., and Merchant, H., 1971, *Material Properties of Cerebral Blood Vessels*, University of Washington, Seattle, WA.

[20] Lee, M. C., and Haut, R. C., 1989, "Insensitivity of Tensile Failure Properties of Human Bridging Veins to Strain Rate: Implications in Biomechanics of Subdural Hematoma," J. Biomech., **22**(6–7), pp. 537–542.

[21] Monea, A. G., Baeck, K., Verbeken, E., Verpoest, I., Sloten, J. V., Goffin, J., and Depreitere, B., 2014, "The Biomechanical Behaviour of the Bridging Vein-Superior Sagittal Sinus Complex With Implications for the Mechanopathology of Acute Subdural Haematoma," J. Mech. Behav. Biomed. Mater., **32**, pp. 155–165.

[22] Bell, E. D., Kunjir, R. S., and Monson, K. L., 2013, "Biaxial and Failure Properties of Passive Rat Middle Cerebral Arteries," J. Biomech., **46**(1), pp. 91–96.

[23] Bell, E. D., Donato, A. J., and Monson, K. L., 2017, "Cerebrovascular Dysfunction Following Subfailure Axial Stretch," J. Mech. Behav. Biomed. Mater., **65**, pp. 627–633.

[24] Van Loon, P., Klip, W., and Bradley, E. L., 1977, "Length-Force and Volume-Pressure Relationships of Arteries," Biorheology, **14**(4), pp. 181–201.

[25] SAE, 1995, "Instrumentation for Impact Test—Part 1: Electronic Instrumentation," *SAE Handbook*, Society of Automotive Engineers, Warrendale, PA, pp. 384–392.

[26] Monson, K. L., Goldsmith, W., Barbaro, N. M., and Manley, G. T., 2003, "Axial Mechanical Properties of Fresh Human Cerebral Blood Vessels," ASME J. Biomech. Eng., **125**(2), pp. 288–294.

[27] Mohan, D., and Melvin, J., 1982, "Failure Properties of Passive Human Aortic Tissue—I: Uniaxial Tension Tests," J. Biomech., **15**(11), pp. 887–902.

[28] Hardy, W. N., Mason, M. J., Foster, C. D., Shah, C. S., Kopacz, J. M., Yang, K. H., King, A. I., Bishop, J., Bey, M., Anderst, W., and Tashman, S., 2007, "A Study of the Response of the Human Cadaver Head to Impact," Stapp Car Crash J., **51**, pp. 17–80.

[29] Morrison, B., Saatman, K. E., Meaney, D. F., and McIntosh, T. K., 1998, "In Vitro Central Nervous System Models of Mechanically Induced Trauma: A Review," J. Neurotrauma, **15**(11), pp. 911–928.

[30] Margulies, S., Thibault, L., and Gennarelli, T., 1990, "Physical Model Simulations of Brain Injury in the Primate," J. Biomech., **23**(8), pp. 823–836.

[31] Meaney, D. F., and Thibault, L. E., 1990, "Physical Model Studies of Cortical Brain Deformation in Response to High Strain Rate Inertial Loading," International IRCOBI Conference on the Biomechanics of Impacts, Bron-Lyon, France, Sept. 12–14, pp. 215–224.

[32] Zhang, J., Song, B., Pintar, F. A., Yoganandan, N., Chen, W., and Gennarelli, T. A., 2008, "How to Test Brain and Brain Simulant at Ballistic and Blast Strain Rates," Biomed. Sci. Instrum., **44**, pp. 129–134.

[33] Zhang, J., Pintar, F. A., Yoganandan, N., Gennarelli, T. A., and Son, S. F., 2009, "Experimental Study of Blast-Induced Traumatic Brain Injury Using a Physical Head Model," Stapp Car Crash J., **53**, pp. 215–227.

[34] Bastien, H., Bouamoul, A., and Rancourt, D., 2014, "Soft Tissue Strain Rates in Side-Blast Incidents," *Defence Research and Development Canada, Valcartier Research Centre*, Quebec City, QC, Canada.

[35] Zhang, L., Makwana, R., and Sharma, S., 2013, "Brain Response to Primary Blast Wave Using Validated Finite Element Models of Human Head and Advanced Combat Helmet," Front. Neurol., **4**, p. 88.

[36] Monson, K. L., Mathur, V., and Powell, D. A., 2011, "Deformations and End Effects in Isolated Blood Vessel Testing," ASME J. Biomech. Eng., **133**(1), p. 011005.